AD-A126 133 SUPERCONDUCTING NIOBIUM THIN-FILM GRADIOMETER TECHNOLOGY PROGRAM(U) TEXAS INSTRUMENTS INC DALLAS EQUIPMENT GROUP S A BUCKNER 14 MAR 83 N00014-82-C-0163 1/1

UNCLASSIFIED F/G 8/14 NL

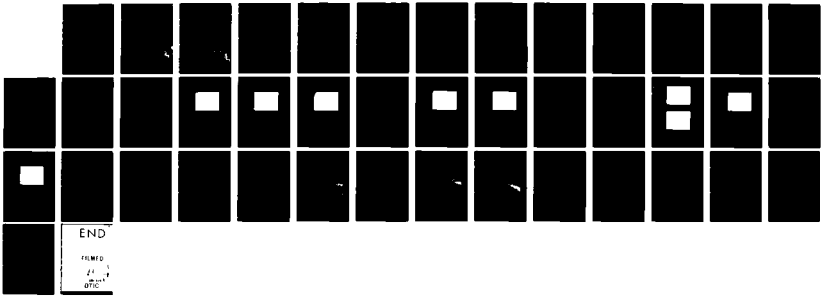

END

FILMED

DTIC

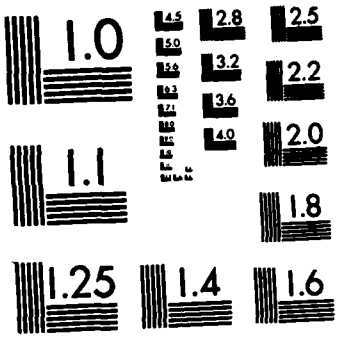

AD A126133

DTIC FILE COPY

FINAL REPORT FOR

SUPERCONDUCTING NIOBIUM THIN-FILM GRADIOMETER TECHNOLOGY PROGRAM

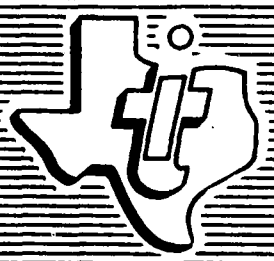

TEXAS INSTRUMENTS
INCORPORATED

FINAL REPORT FOR

SUPERCONDUCTING NIOBIUM THIN-FILM GRADIOMETER TECHNOLOGY PROGRAM

Prepared For:

Defense Advanced Research
Projects Agency
1400 Wilson Boulevard
Arlington, VA 22209

Prepared By:

Texas Instruments Incorporated
Equipment Group
P.O. Box 225012, M/S 43
Dallas, TX 75265

14 March 1983

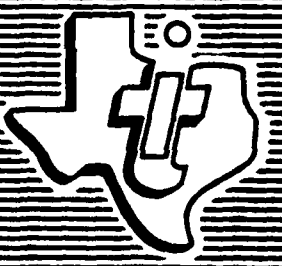

TEXAS INSTRUMENTS
INCORPORATED

SECURITY CLASSIFICATION OF THIS PAGE (When Data Entered)

REPORT DOCUMENTATION PAGE

READ INSTRUCTIONS BEFORE COMPLETING FORM

1. REPORT NUMBER	2. GOVT ACCESSION NO. / 3. RECIPIENT'S CATALOG NUMBER
4. TITLE (and Subtitle): FINAL REPORT FOR SUPERCONDUCTING NIOBIUM THIN-FILM GRADIOMETER TECHNOLOGY PROGRAM	5. TYPE OF REPORT & PERIOD COVERED: Final Report 4 Jan 1982 - 17 Jan 1983
	6. PERFORMING ORG. REPORT NUMBER
7. AUTHOR(s): Spencer A. Buckner	8. CONTRACT OR GRANT NUMBER(s): N00014-82-C-0163
9. PERFORMING ORGANIZATION NAME AND ADDRESS: Texas Instruments Incorporated, Equipment Group, P.O. Box 225012, M/S 43, Dallas, TX 75265	10. PROGRAM ELEMENT, PROJECT, TASK AREA & WORK UNIT NUMBERS
11. CONTROLLING OFFICE NAME AND ADDRESS: Defense Advanced Research Projects Agency, 1400 Wilson Boulevard, Arlington, VA 22209	12. REPORT DATE: 14 March 1983
	13. NUMBER OF PAGES: 34
14. MONITORING AGENCY NAME & ADDRESS (if different from Controlling Office)	15. SECURITY CLASS. (of this report): UNCLASSIFIED
	15a. DECLASSIFICATION/DOWNGRADING SCHEDULE

16. DISTRIBUTION STATEMENT (of this Report)

Approved for public release; distribution unlimited.

17. DISTRIBUTION STATEMENT (of the abstract entered in Block 20, if different from Report)

18. SUPPLEMENTARY NOTES

19. KEY WORDS (Continue on reverse side if necessary and identify by block number)

SQUID, magnetometer, gradiometer, superconductivity, Josephson junction.

20. ABSTRACT (Continue on reverse side if necessary and identify by block number)

Dc SQUIDs with 2.5 μm square niobium-aluminum oxide-niobium tunnel junctions and titanium resistive shunts have been fabricated. The SQUID inductance was 0.9 nH, and the shunt resistors were approximately 10 ohms. With the SQUIDs operated in a small-signal amplifier mode the white noise of the SQUIDs was measured to have a minimum value of $2.8 \times 10^{-5}\ \phi_o/\sqrt{Hz}$ at 20 kHz. Low-frequency noise was measured from 0.005 to 2 Hz with the SQUIDs operated in a closed-loop negative-feedback mode. A straight line with a slope of -20 db/

DD FORM 1 JAN 73 1473 EDITION OF 1 NOV 65 IS OBSOLETE

SECURITY CLASSIFICATION OF THIS PAGE (When Data Entered)

decade (1/f frequency dependence) fits the data below 0.5 Hz. This line intersects a horizontal line through the white noise at about 1.6 Hz.

A design was completed of a thin-film gradiometer with one-inch square pickup loops, a baseline of 1.1 inches, and a 50-turn input coil, which will fit on a 3-inch diameter silicon wafer. The sensitivity of this gradiometer was predicted to be 3×10^{-14} (T/m)/$\sqrt{Hz}$ = 3×10^{-5} (γ/m)/$\sqrt{Hz}$. Fabrication of this completely integrated thin-film gradiometer made only of refractory metals should provide an excellent means of predicting the achievable sensitivity and balance of an airborne magnetic gradiometer.

Summary

The principal candidate for the detection of magnetic field gradients produced by ships and submarines is the superconducting gradiometer which uses a SQUID (superconducting quantum interference device) as the detector element. The fundamental sensitivity of a gradiometer is determined by the following: (1) SQUID noise level, (2) size of pickup loops, and (3) the coupling between the pickup loops and the SQUID. A critical performance factor is gradiometer balance. Balance is defined as the gradiometer output signal, when a uniform magnetic field is applied to the sensor, divided by the magnitude of the applied field. A completely integrated thin-film gradiometer should provide the optimum sensitivity and balance for this application. This effort was the first phase of a program to build such a device using only refractory thin films to achieve as rugged a device as possible.

DC SQUIDs with 2.5 μm square niobium-aluminum oxide-niobium tunnel junctions and titanium resistive shunts have been fabricated. The SQUID inductance was 0.9 nH, and the shunt resistors were approximately 10 ohms. With the SQUIDs operated in a small-signal amplifier mode the white noise of the SQUIDs was measured to have a minimum value of $2.8 \times 10^{-5}\ \phi_0/\sqrt{Hz}$ at 20 kHz. Low frequency noise was measured from 0.05 to 2 Hz with the SQUIDs operated in a closed-loop negative-feedback mode. A straight line with a slope of -20 db/decade (1/f frequency dependence) fits the data below 0.5 Hz. This line intersects a horizontal line through the white noise at about 1.6 Hz.

A design was completed of a thin-film gradiometer with one-inch square pickup loops, a baseline of 1.1 inches, and a 50-turn input coil, which will

fit on a 3-inch diameter silicon wafer. The sensitivity of this gradiometer was predicted to be 3×10^{-14} (T/m)/$\sqrt{\text{Hz}}$ = 3×10^{-5} (γ/m)/$\sqrt{\text{Hz}}$. Fabrication of this completely integrated thin-film gradiometer made only of refractory metals should provide an excellent means of predicting the achievable sensitivity and balance of an airborne magnetic gradiometer.

Table of Contents

	Page
Introduction	1
Fabrication of superconducting tunnel junctions	2
Vacuum system	2
Photolithographic masks	2
Tunnel junctions	3
Fabrication of resistively-shunted tunnel junctions	12
Fabrication of SQUIDs	15
SQUID electrical characteristics	15
Current-voltage characteristics and modulation of critical current	15
Dependence of SQUID voltage on magnetic flux	19
Dependence of $dv/d\phi$ and dv/di on magnetic flux	21
White noise in the SQUID	23
Low-frequency noise in the SQUID	24
Gradiometer design	29
Conclusions and recommendations	32
References	33

Final Report for Superconducting Niobium Thin-Film Gradiometer Technology Program

Introduction.

The objective of this program was to develop the technology for the preparation of superconducting niobium thin-film gradiometers. The following tasks were completed during the contract period:

(1) fabrication of superconducting tunnel junctions with two different tunnel-barrier materials and both electrodes made of niobium

(2) fabrication of niobium-niobium tunnel junctions with normal-metal shunt resistors, producing nonhysteretic current-voltage characteristics

(3) fabrication of dc SQUIDs using these resistively shunted tunnel junctions

(4) measurement of the electrical characteristics of these SQUIDs

  (a) bias current, i, versus SQUID voltage, v

  (b) modulation of SQUID critical current, I_c, by magnetic flux, ϕ, in the SQUID

  (c) v versus ϕ

  (d) $dv/d\phi$ versus ϕ

  (e) differential resistance, dv/di, versus ϕ

(5) measurement of the white noise in the SQUID as a function of flux with the SQUID in a small-signal amplifier mode

(6) measurement of low-frequency noise in the SQUID with the SQUID incorporated in a closed-loop negative feedback system

(7) design of a complete gradiometer with one-inch square pickup loops, a baseline of 1.1 inches, and a 50-turn input coil, which will fit on a 3-inch diameter silicon wafer.

Each of these seven areas will be discussed separately in the remainder of the report.

Fabrication of superconducting tunnel junctions.

Vacuum system.

The vacuum system used to make the niobium-niobium tunnel junctions described in this report is a Sloan sputter deposition system pumped by an oil diffusion pump. This system will pump down to approximately 2×10^{-7} Torr in the chamber in several hours. The system has ports for three magnetron sputter guns with cylindrical targets. Two sputter guns are in place while the third port is blanked off. When the substrate is sputter cleaned or sputter oxidized, it is positioned under this third port. Niobium deposition rates of approximately 2000 Å/min and critical temperatures close to that of bulk niobium for nominal thicknesses of 1000 - 3000 Å are achieved in this system. Pressures during sputter deposition or sputter cleaning are measured with an MKS Instruments model 220 capacitance manometer with digital readout over four decades: 0.0001 to 1 Torr. Rf power during sputter cleaning or oxidation is supplied by a 500 watt Henry power supply.

Photolithographic masks.

Photolithographic masks used during this work were designed to make "cross-type" junctions of three different sizes: 2.5 μm x 2.5 μm, 5 μm x 5 μm, and 250 μm x 250 μm. There are ten 2.5-μm junctions, four 5-μm junctions, and two 250-μm junctions. The 2.5-μm and 5-μm junctions are in two parallel rows

of seven junctions each. The junctions in each row are 0.5 mm apart, and the two rows are 5 mm apart. The 250-μm junctions are halfway between the rows of smaller junctions and are 6 mm apart. The junctions are connected in parallel electrically so that each junction can be tested separately without sending current through other junctions. This design is shown schematically in Figure 1. The masks also contain four dc SQUIDs, each incorporating two 2.5-μm cross-type junctions. The design of the SQUIDs will be discussed in greater detail in the section on SQUID fabrication.

A test fixture with spring-loaded probes was used to make electrical contact with pads on the substrates. This fixture was mounted on a probe which could be lowered into a liquid helium Dewar for testing.

Tunnel junctions.

Superconducting tunnel junctions with niobium electrodes and two different tunnel barrier materials have been made during the contract period. The two tunnel barrier materials were aluminum oxide and silicon oxide. The techniques that produced the best results for each of these barrier materials will be described.

The niobium base electrode was dc sputtered in the Sloan sputter deposition system on oxidized 3-inch diameter silicon wafers. Typical thicknesses of the films were 1000 - 1200 Å. A photoresist pattern was developed on the surface of the niobium film, and it was plasma etched in a mixture of 27% oxygen and the balance carbon tetrafluoride. Plasma etching the pattern in this gas mixture produced tapered edges on the niobium films. A lift-off photoresist pattern was then applied to the substrate. An undercut photoresist profile was created by soaking the photoresist in

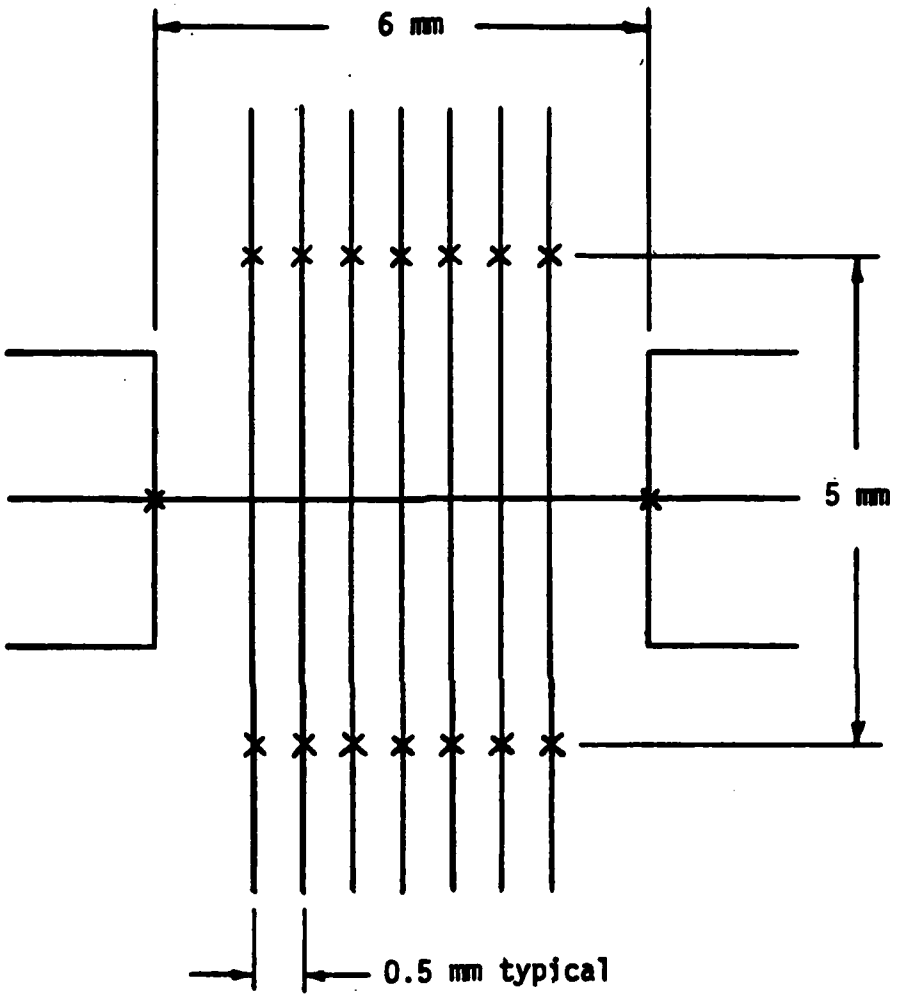

Figure 1. Schematic diagram of central part of photolithographic masks for junction fabrication.

o-dichlorobenzene for approximately ten minutes after exposure of the pattern. The surface of the niobium film was sputter cleaned in argon at a pressure of 0.010 Torr. The peak-to-peak rf voltage was approximately 450 V. The substrates were sputter cleaned for 15 minutes. Aluminum was then rf sputtered onto the substrate at a very low power in 0.010 Torr of oxygen. A typical time for this deposition was 10 seconds. A sputter oxidation step followed in 0.038 Torr of argon plus 0.002 Torr of oxygen. The peak-to-peak rf voltage was approximately 170 V. This step lasted typically one minute. A 1500 Å film of niobium was then dc sputtered onto the substrate to complete the junctions. The niobium upper electrode pattern was formed by dissolving the photoresist pattern in acetone and lifting off the unwanted parts of the upper niobium film.

The fabrication process for junctions made with silicon-oxide barriers was similar to that described above for aluminum-oxide barriers. The same sputter-cleaning step was used, but it was followed by rf sputtering silicon, instead of aluminum, in 0.010 Torr of oxygen. A typical time for this deposition was 50 seconds. No sputter oxidation step was used for the silicon-oxide barrier junctions. Instead, the silicon-oxide deposition step was followed immediately by dc sputter deposition of the niobium upper electrode. The upper electrode pattern was again formed by the lift-off technique. Since silicon sputters slower than aluminum, it is easier to control the oxide thickness with the silicon-oxide barriers. Our highest quality niobium-niobium junctions were made with silicon-oxide barriers.

Two parameters have been used to characterize the quality of our superconducting tunnel junctions. The first is the ratio of the subgap resistance,

R_s, to the normal-state resistance, R_n. We have defined the subgap resistance for our junctions to be the ratio of the voltage and current in the junction at 1.5 mV (approximately half the superconducting energy gap):

$$R_s = (1.5\ \text{mV})/(I(1.5\ \text{mV}))$$

The normal-state resistance is defined to be the ratio of the voltage and current at 4.0 mV (above the energy gap):

$$R_n = (4.0\ \text{mV})/(I(4.0\ \text{mV}))$$

The second parameter is V_m, the product of the junction critical current, I_c, and the subgap resistance, R_s, defined above.

BCS theory predicts that the critical current, I_c, is related to the normal-state resistance, R_n, by the relation:[1]

$$I_c = (\pi\Delta(T)/2eR_n)\ \tanh\ (\Delta(T)/2kT)$$

where $\Delta(T)$ is the temperature-dependent energy-gap parameter. This relation predicts that the I_cR_n product is determined by the superconducting energy gap and the temperature. For $\Delta(T)/e = 1.5$ mV and $T = 4.2$ K this expression gives:

$$I_cR_n = 2.4\ \text{mV}$$

In practice the measured value of I_c is reduced by strong coupling and/or proximity effects.[2]

In general, the single-particle tunneling current can be calculated from an expression which must be integrated numerically. Analytic results have been obtained for some special cases, however. One special case is for a tunnel junction with identical superconductors on each side of the barrier, $kT \ll \Delta$, and $eV < 2\Delta$.[3] For $T = 4.2$ K, $kT/\Delta = 0.24$ so that the analytic expression is fairly accurate. This expression predicts that:

$V_m = I_c R_s = 95$ mV

and

$R_s/R_n = V_m/I_c R_n = 40$

The best values of these parameters (that is, the largest values of R_s/R_n and V_m) that we have obtained for aluminum-oxide barrier junctions are for a 250-μm junction:

I_c = 33 μA

R_s = 83 ohms

R_n = 21 ohms

R_s/R_n = 3.92

V_m = 2.7 mV

Values of these parameters for 2.5-μm junctions on the substrate which had the highest-quality junctions of this size with aluminum-oxide barriers are:

I_c = 0 for all 2.5-μm junctions on this substrate

R_s = 2300 - 5000 ohms

R_n = 730 - 1290 ohms

R_s/R_n = 2.25 - 3.88 (average value = 3.35)

Values for 5-μm junctions on this substrate are:

I_c = 0 for all 5-μm junctions

R_s = 790 - 940 ohms

R_n = 230 - 260 ohms

R_s/R_n = 3.41 - 3.66 (average value = 3.59)

There has been a tendency for the larger-area junctions on each substrate to be of higher quality than the smaller ones. At the present time we have no explanation for this observation. One would usually expect larger-area junctions to be more difficult to make since there should be a greater

likelihood for pinholes or shorts through the barrier. A possible explanation is that the edges of the junctions (where the films overlap) play a bigger role when the area of the junctions is small. Plasma etching of the base electrode should produce tapered edges on these films and thereby minimize problems where the films cross, however.

Preliminary work fabricating silicon-oxide barrier junctions produced higher-quality junctions than we had obtained with aluminum-oxide barriers. The best silicon-oxide barrier junction was 250 μm square and had the following parameter values:

I_c = 0

R_s = 2100 ohms

R_n = 480 ohms

R_s/R_n = 4.45

Figures 2, 3, and 4 show current-voltage characteristics for the junctions described above. These junctions are entirely adequate for use in SQUIDs for magnetometer applications since they must be resistively shunted to get rid of the hysteresis in the I-V characteristic. Excess current below the energy-gap voltage (producing low values of R_s/R_n and V_m), therefore, is not important. Reproducibility and the ability to obtain critical currents of the desired value are the most important aspects of junction fabrication for this application.

For comparison the best values of these parameters that we have obtained for niobium-niobium oxide-lead junctions (which are easier to make than niobium-insulator-niobium junctions) are:

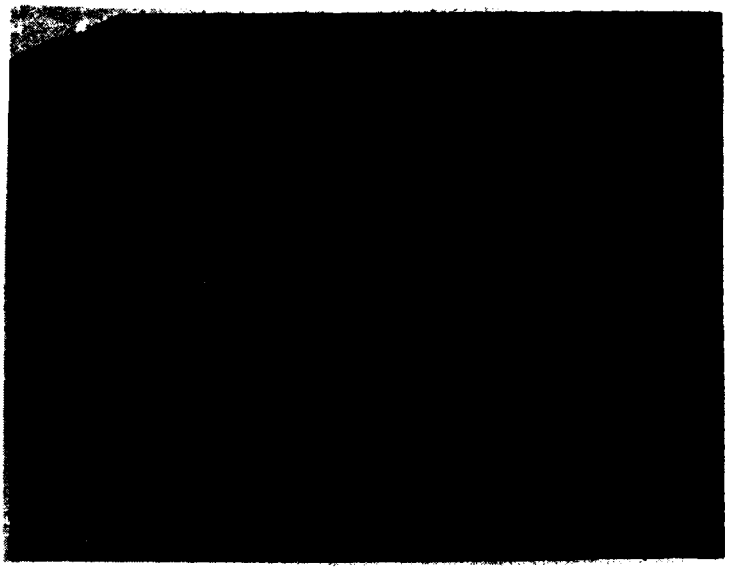

Figure 2. Current-voltage characteristic of 250 μm x 250 μm niobium-aluminum oxide-niobium tunnel junction. I_c = 33 μA, R_s/R_n = 3.92.

Figure 3. Current-voltage characteristic of 2.5 μm x 2.5 μm niobium-aluminum oxide-niobium tunnel junction. $I_c = 0$, $R_s/_{n} = 3.88$.

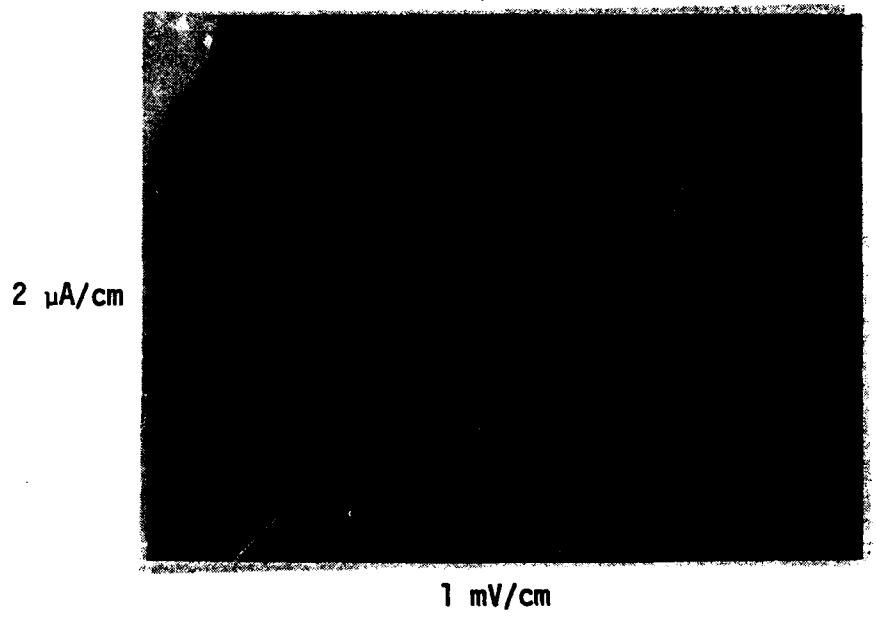

Figure 4. Current-voltage characteristic of 250 μm x 250 μm niobium-silicon oxide-niobium tunnel junction. $I_c = 0$, $R_s/R_n = 4.45$.

best R_s/R_n = 20

best V_m = 26 mV

The best values of R_s/R_n and V_m reported by others for all-niobium tunnel junctions are summarized in the table below:

	Bell Laboratories[4]	IBM[5]	Sperry Research Center[6]
best R_s/R_n	23	8.6	8.9
best V_m	35 mV	13 mV	12 mV

Fabrication of resistively-shunted tunnel junctions.

Titanium shunt resistors were added to half the junctions and to all four SQUIDs on each of three separate substrates. Our procedure was to test junctions and SQUIDs immediately after the junctions were made (before shunt resistors were added). If the critical currents of the SQUIDs were in the proper range, then the shunts were added. The additional processing consisted of application of a photoresist lift-off pattern to the substrates, a sputter-cleaning step similar to that used in making the junctions, and dc sputter deposition of a 3000 Å film of titanium. This resulted in 10-ohm shunt resistors. Figures 5 and 6 show I-V characteristics for 2.5-μm and 5-μm junctions after addition of shunt resistors.

The overall quality of the junctions did not change appreciably during this additional processing, but the critical currents were affected. We have observed increases by factors of 3 to 6. These increases are probably caused by heating of the substrates during the additional processing. We tried to

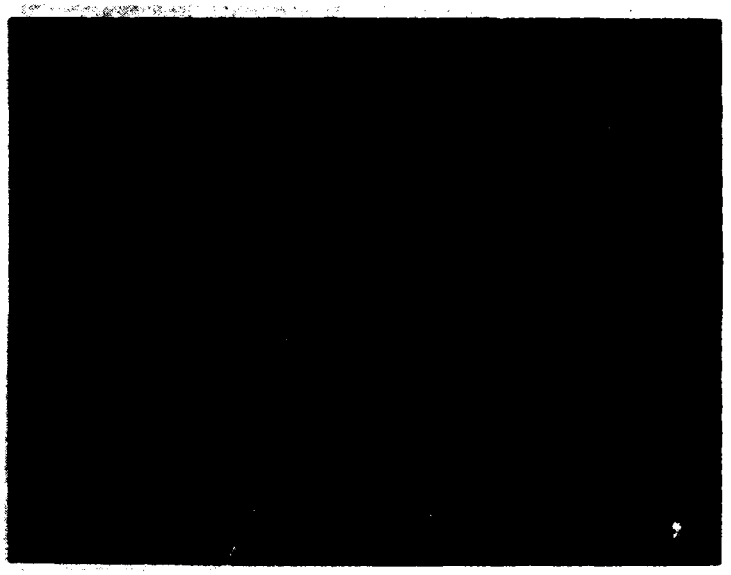

Figure 5. Current-voltage characteristic of 2.5 μm x 2.5 μm niobium-aluminum oxide-niobium tunnel junction with titanium shunt resistor. I_c = 2.5 μA.

Figure 6. Current-voltage characteristic of 5 μm x 5 μm niobium-aluminum oxide-niobium tunnel junction with titanium shunt resistor. I_c = 3.8 μA.

minimize heating of the junctions after they were formed by not baking the photoresist for the shunt resistor pattern. However, increases in the critical current still occurred. The problem is probably the heating which occurs during the sputter-cleaning step which immediately precedes deposition of the titanium film.

Fabrication of SQUIDs.

Dc SQUIDs with resistively-shunted tunnel junctions were obtained automatically when titanium shunt resistors were added to single junctions since SQUIDs and junctions were formed at the same time on the substrates. We have obtained working SQUIDs on three different substrates. Each of these substrates has four separate SQUIDs. Figure 7 shows the SQUID geometry. The SQUID inductance is approximately 0.9 nH, and the shunt resistors are approximately 10 ohms. The junctions in all the SQUIDs are 2.5 μm square. Critical currents for these SQUIDs range from 3 to 15 μA. A magnetic field was applied to the SQUID by sending a current through the film just to the right of the SQUID. Figure 8 shows photographs of a SQUID with 2.5-μm junctions and titanium shunt resistors.

SQUID electrical characteristics.

All the electrical measurements described below were conducted with the SQUID and associated electronics inside a shielded room. In addition the Dewar containing the SQUID was placed inside a two-layer mu-metal can to shield against low-frequency magnetic signals.

Current-voltage characteristics and modulation of critical current.

Figure 9 shows the I-V characteristic of a SQUID before addition of titanium shunt resistors. The curve is hysteretic with a critical current

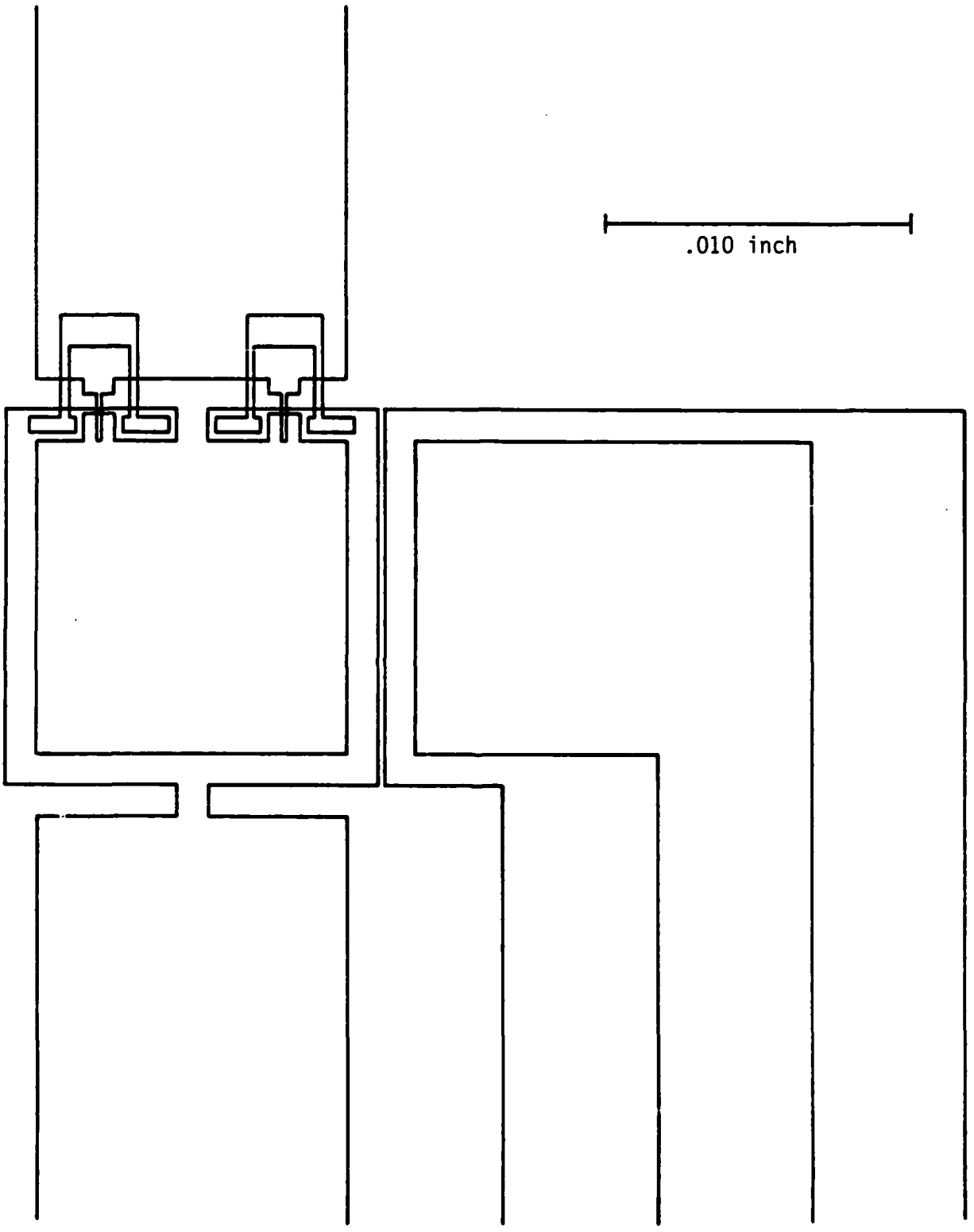

Figure 7. Geometry of dc SQUID with two 2.5-μm tunnel junctions.

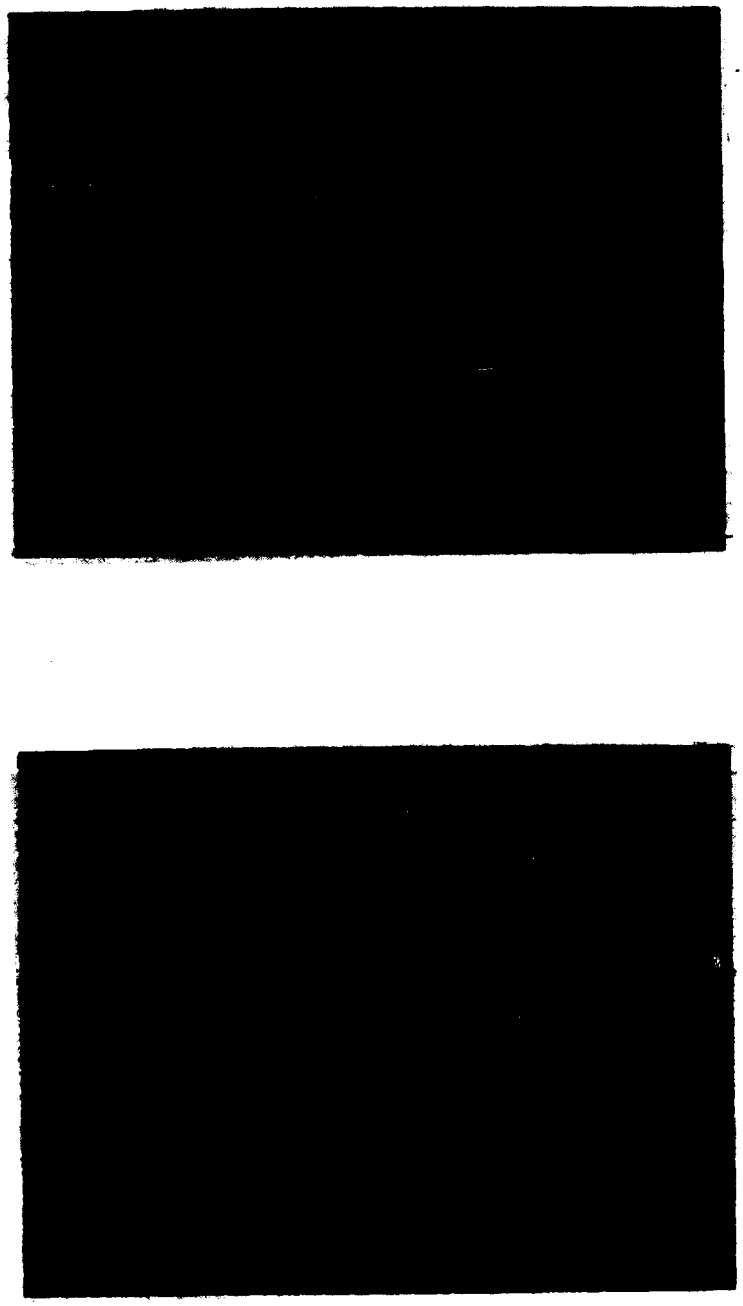

Figure 8. Photographs of dc SQUID with two 2.5-μm tunnel junctions and titanium shunt resistors.

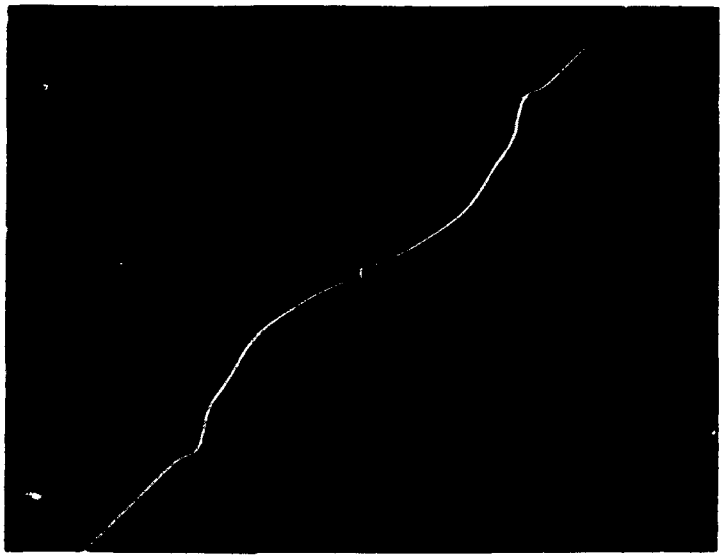

Figure 9. Current-voltage characteristic of dc SQUID before addition of titanium shunt resistors. I_c = 1.1 μA. (SQUID #2, substrate #2, made on 7-27-82)

of approximately 1.1 μA. After addition of 10-ohm titanium shunt resistors the I-V curve is nonhysteretic. Figure 10 shows I-V curves for small voltages for this same SQUID with shunt resistors. The larger critical current corresponds to an integral number of flux quanta being coupled to the SQUID. The smaller critical current corresponds to a half-integral number of flux quanta coupled to the SQUID. Modulation of the critical current has ranged from 10 to 41% for different SQUIDs with different critical currents. In general, the smaller the value of the parameter $2LI_c/\phi_0$, the greater the modulation percent of the critical current. This is what we observed.

Dependence of SQUID voltage on magnetic flux.

When the SQUIDs were biased with a constant-current supply, modulation of the critical current with a magnetic field produced voltage changes across the SQUIDs of as much as 6 μV peak-to-peak. Calculations show that an appropriate formula for the voltage modulation is:

$$\Delta V = R_d \phi_0 / 2L$$

where R_d is the differential resistance of the SQUID at the bias point, $\phi_0 = 2.07 \times 10^{-15}$ T·m^2 is the flux quantum, and L is the SQUID inductance. For our SQUIDs L = 0.9 nH, and R_d varied from 7 to 10 ohms, depending on the magnetic flux linking the SQUID. An average value of 8.5 ohms should produce a ΔV of approximately 10 μV. The lower values of ΔV which we observed are probably due to contact resistance between the niobium films and the spring-loaded probes used to make contact to them. The voltage across the SQUID drives current through an impedance-matching transformer at room temperature. Extra resistance in this circuit reduces the current flowing in the transformer primary and therefore reduces the voltage measured across the secondary. Use

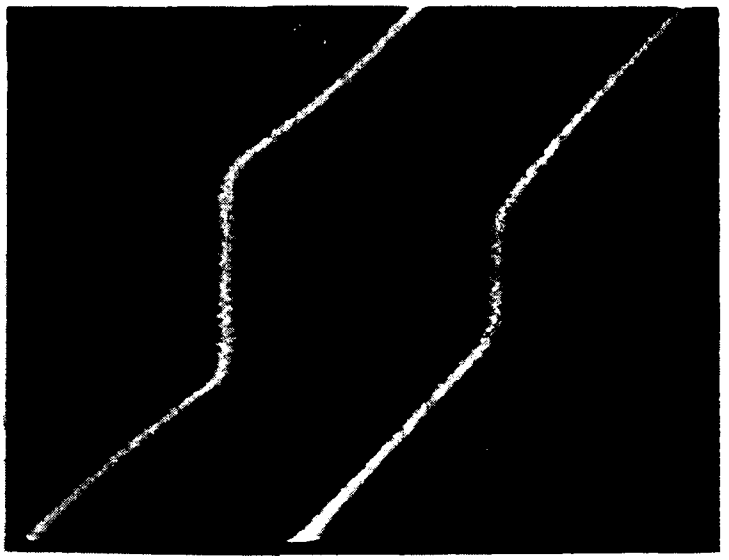

Figure 10. Current-voltage characteristics of dc SQUID for small voltages after addition of titanium shunt resistors. Curves show effect of magnetic field on critical current of SQUID. I_c = 3.0 μA, modulation = 41%. (SQUID #2, substrate #2, made on 7-27-82)

of the spring-loaded probes made testing easy and fast but is not the best solution. A better solution is to ultrasonically bond aluminum wires to the niobium films. This will be done on the next generation of SQUIDs that we make.

Curve (a) in Figure 11 shows a plot of SQUID voltage as a function of magnetic flux linking the SQUID. A square-wave current generator was used to bias the SQUID. The current alternated between zero and the dc value where the SQUID was most sensitive to changes in magnetic flux. The voltage across the SQUID was applied to the input of an EG&G Princeton Applied Research model 119 preamplifier which was installed in a PAR model 124A lock-in amplifier. The preamplifier was operated in the transformer mode to give the best impedance matching between the SQUID and the preamplifier. A slowly-varying magnetic signal was applied to the SQUID. The phase-sensitively detected signal at the output of the lock-in (using the current modulation as a reference) was plotted on an X-Y plotter as a function of the applied magnetic signal.

Dependence of $dv/d\phi$ and dv/di on magnetic flux.

Curves (b) and (c) in Figure 11 show plots of $dv/d\phi$ and dv/di as a function of magnetic flux. Curve (b) is useful because flux noise in the SQUID is the ratio of the voltage noise to $dv/d\phi$. Curve (c) is interesting because from it one can determine if maxima in voltage noise correspond with maxima in dv/di, the differential resistance. Curve (b) was obtained by using a constant-current bias and applying a small-amplitude flux signal to the SQUID. The voltage across the SQUID was applied to the input of the lock-in amplifier, and the output recorded as a function of the slowly-varying flux

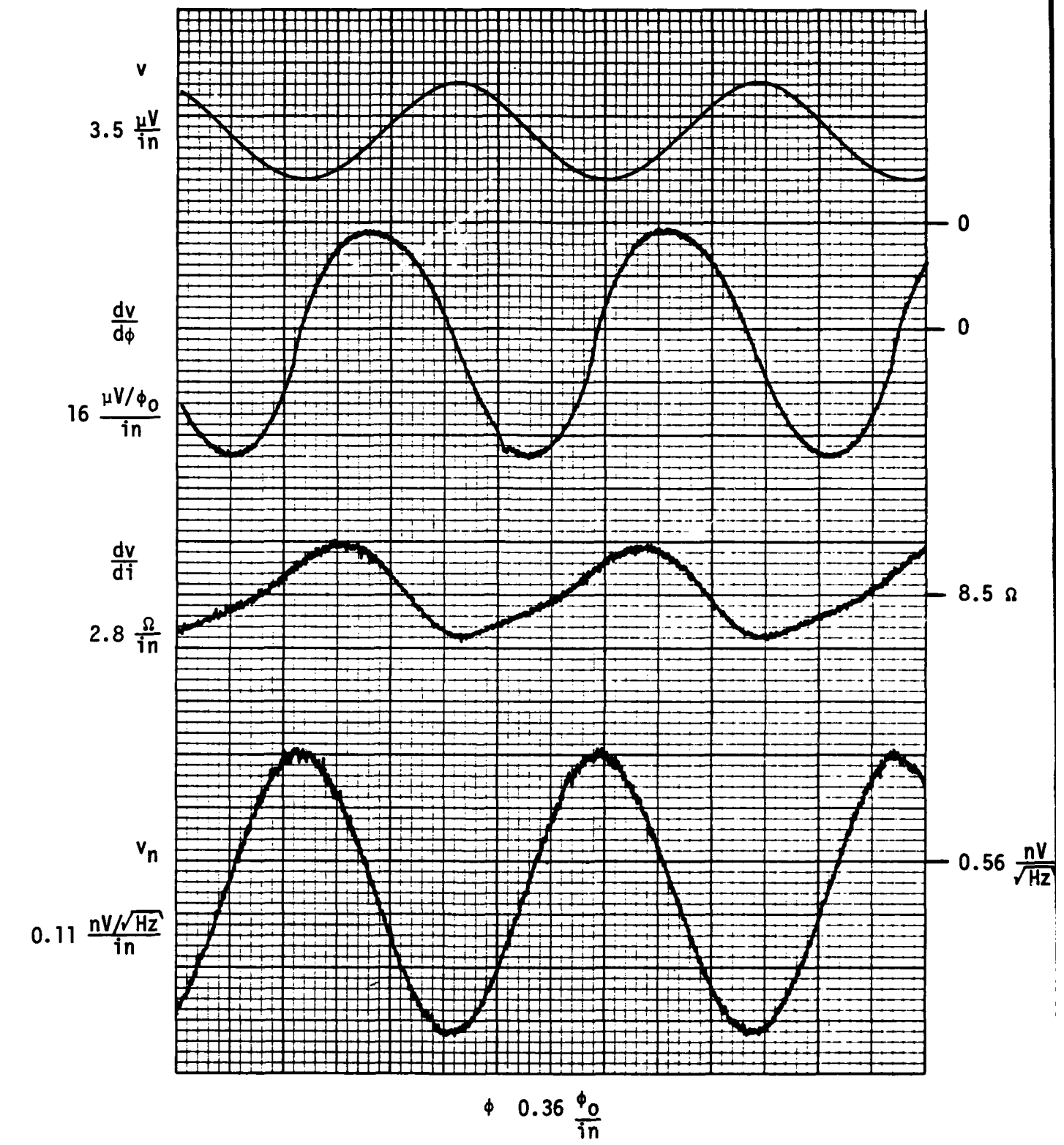

Figure 11. Electrical characteristics of dc SQUID as a function of magnetic flux. (SQUID #3, substrate #3, made on 8-24-82)

signal. The flux modulation used in this case was $9 \times 10^{-3}\ \phi_0$ peak-to-peak. Curve (c) was obtained by adding a small amplitude current modulation to a constant-current bias and recording the output of the lock-in amplifier as a function of the slowly-varying flux signal. The constant-current bias used in this case was 14 μA, and the current modulation was 25 nA peak-to-peak.

White noise in the SQUID.

Curve (d) in Figure 11 shows a plot of the voltage noise in a 2 kHz bandwidth centered at 20 kHz. The SQUID was biased with a constant-current source, and the voltage across the SQUID was applied to the input of the PAR 119 preamplifier in the transformer mode. This transformer was measured to have a noise temperature of 18 K at 20 kHz for a 10-ohm source resistance. The PAR 124A lock-in amplifier was used in the ac-voltmeter mode to measure the total voltage noise of SQUID plus transformer as a function of the slowly-varying flux signal. The transformer voltage noise in a 2 kHz bandwidth centered at 20 kHz, referred to the input of the transformer, was measured to be $2.0 \times 10^{-17}\ V^2$ for a 10-ohm source resistance. The total voltage noise plotted in curve (d) varies from 2.9 to $9.0 \times 10^{-16}\ V^2$. The voltage noise of the transformer, therefore, was approximately 3% of the total voltage noise measured and can be neglected. It is interesting to observe that minima in the dv/di versus flux curve occur at the same values of flux as the minima in voltage noise, but that maxima in the dv/di curve do not occur at the same places as the maxima in the voltage noise. We do not have an explanation for this behavior at the present time.

The maxima and minima of the $dv/d\phi$ curve, curve (b) in Figure 11, occur at $(n + 0.21)\phi_0$ and $(n + 0.75)\phi_0$, respectively. The values of $dv/d\phi$ at these

points are 14.4 $\mu V/\phi_0$ and -19.2 $\mu V/\phi_0$. The values of the voltage noise at these values of flux are 0.55 nV/$\sqrt{Hz}$ and 0.54 nV/$\sqrt{Hz}$. Calculating the flux noise at these two points gives $3.8 \times 10^{-5}\ \phi_0/\sqrt{Hz}$ and $2.8 \times 10^{-5}\ \phi_0/\sqrt{Hz}$, respectively. Between these points the flux noise increases to high values at $n\phi_0$ and $(n + 0.5)\phi_0$, where $dv/d\phi$ goes to zero.

Low-frequency noise in the SQUID.

To measure low-frequency noise we have operated the SQUIDs in a closed-loop negative feedback mode. To do this a 20 kHz flux modulation signal is applied to the SQUID, and the output of the lock-in amplifier is fed back through a resistor to the modulation coil. In this mode the SQUID locks on to one of the voltage-versus-flux maxima or minima, depending on the sign of the feedback signal. Voltage changes across the feedback resistor are then proportional to changes in flux in the SQUID.

Voltage noise across the feedback resistor was measured in two different ways. One way was to apply this signal directly to the input of a Hewlett-Packard 5420A digital signal analyzer located outside the shielded room. One problem with this method was that the digital signal analyzer caused noise to be added to the voltage signal across the SQUID, as observed on an oscilloscope. In addition the amplitude of the signal was reduced somewhat. Data were taken this way, however, and the results are shown in Figure 12. The vertical scale is plotted in db with zero db equal to an rms noise of $1\ \phi_0/\sqrt{Hz}$. The horizontal scale is proportional to the logarithm of the frequency and extends from approximately 0.1 to 10 Hz at the right edge of the graph. The white noise is approximately -89 db, which corresponds to $3.5 \times 10^{-5}\ \phi_0/\sqrt{Hz}$.

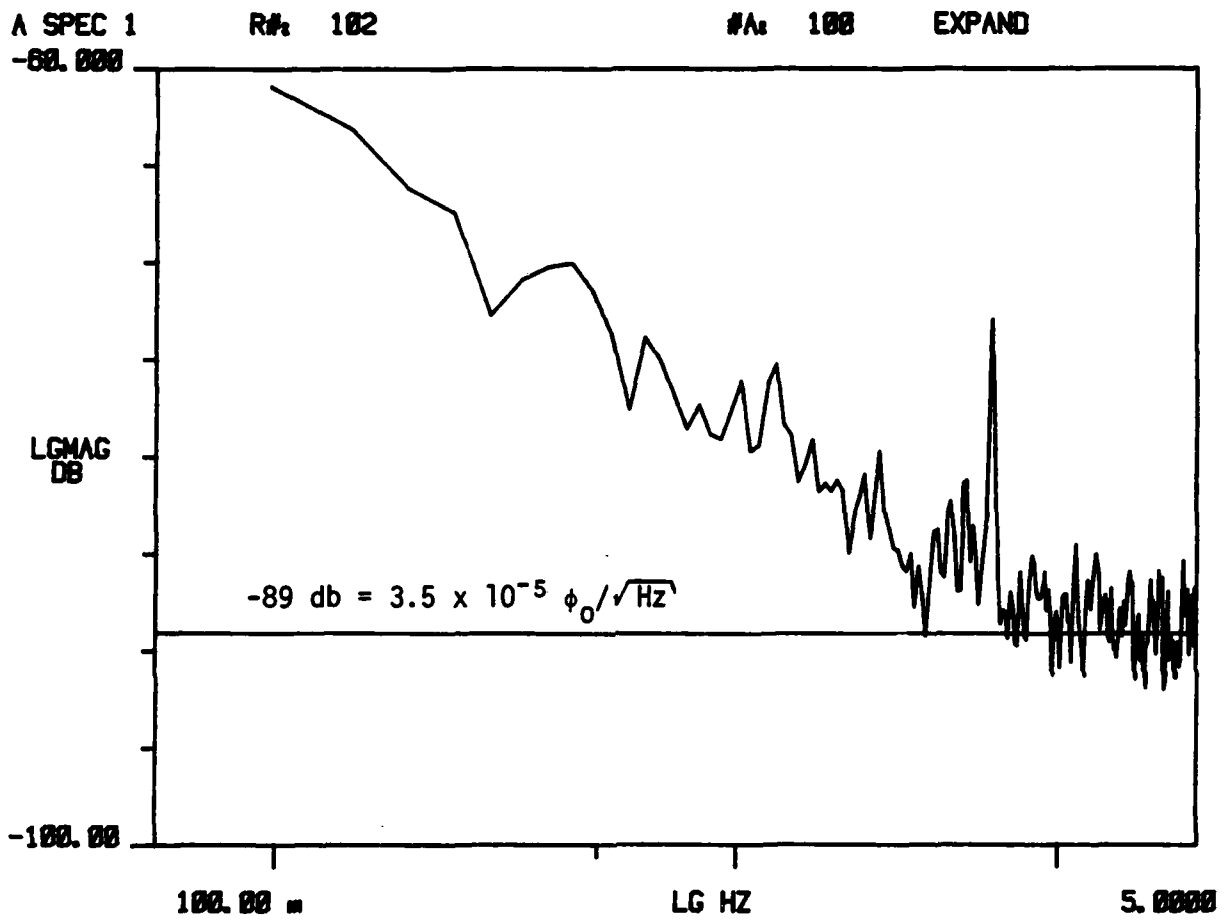

Figure 12. Noise spectrum of dc SQUID measured from 0.1 to 10 Hz. (SQUID #1, substrate #2, made on 7-27-82)

The second method used to measure the low-frequency noise was to record the voltage noise across the feedback resistor on a Honeywell 101 16-channel tape recorder located outside the shielded room. The data recorded on the tape could then be analyzed later using the digital signal analyzer. This method avoided connecting the signal analyzer directly to the SQUID electronics. It was noticed, however, that connection of the tape recorder to the output of the lock-in amplifier slightly reduced the amplitude of the SQUID voltage signal. The signal did not appear to be noisier as was the case with the digital signal analyzer. Plots of data taken this way are shown in Figures 13 and 14. The white noise for this SQUID is approximately -87 db, which corresponds to $4.5 \times 10^{-5}\ \phi_0/\sqrt{\text{Hz}}$. A straight line with a slope of -20 db/decade (1/f frequency dependence) has been fit to the data below 0.5 Hz. This line fits the data fairly well and intersects a horizontal line through the white noise at about 1.6 Hz.

Figures 11 and 13 contain noise data for the same SQUID in two different modes of operation. Figure 11, curve (d), shows the white noise of the SQUID, with the feedback loop open, as a function of flux. As was discussed above, the noise has two minima occurring at flux values of $(n + 0.21)\phi_0$ and $(n + 0.75)\phi_0$. The values of the noise at these two values of flux are 3.8 and $2.8 \times 10^{-5}\ \phi_0/\sqrt{\text{Hz}}$, respectively. Figure 13 shows the noise of the SQUID operating with the feedback loop closed. The SQUID is driven by a sinusoidal modulation flux with an amplitude of approximately $\phi_0/4$. In this mode of operation the flux noise is effectively the average over the flux bias points swept out by the modulation. The bias signal is in regions of relatively high values of $dv/d\phi$ most of the time so that the noise is not degraded

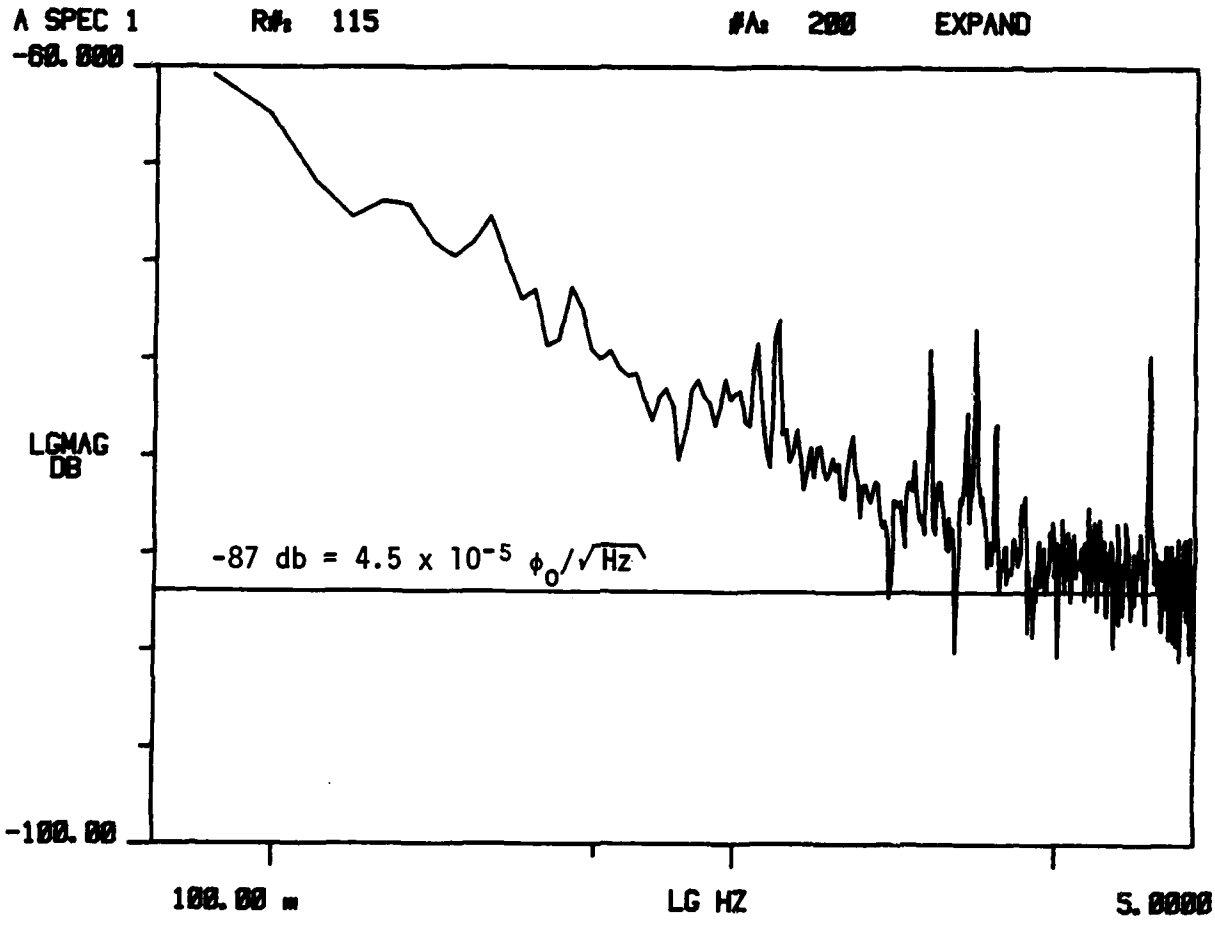

Figure 13. Noise spectrum of dc SQUID measured from 0.1 to 10 Hz. (SQUID #3, substrate #3, made on 8-24-82)

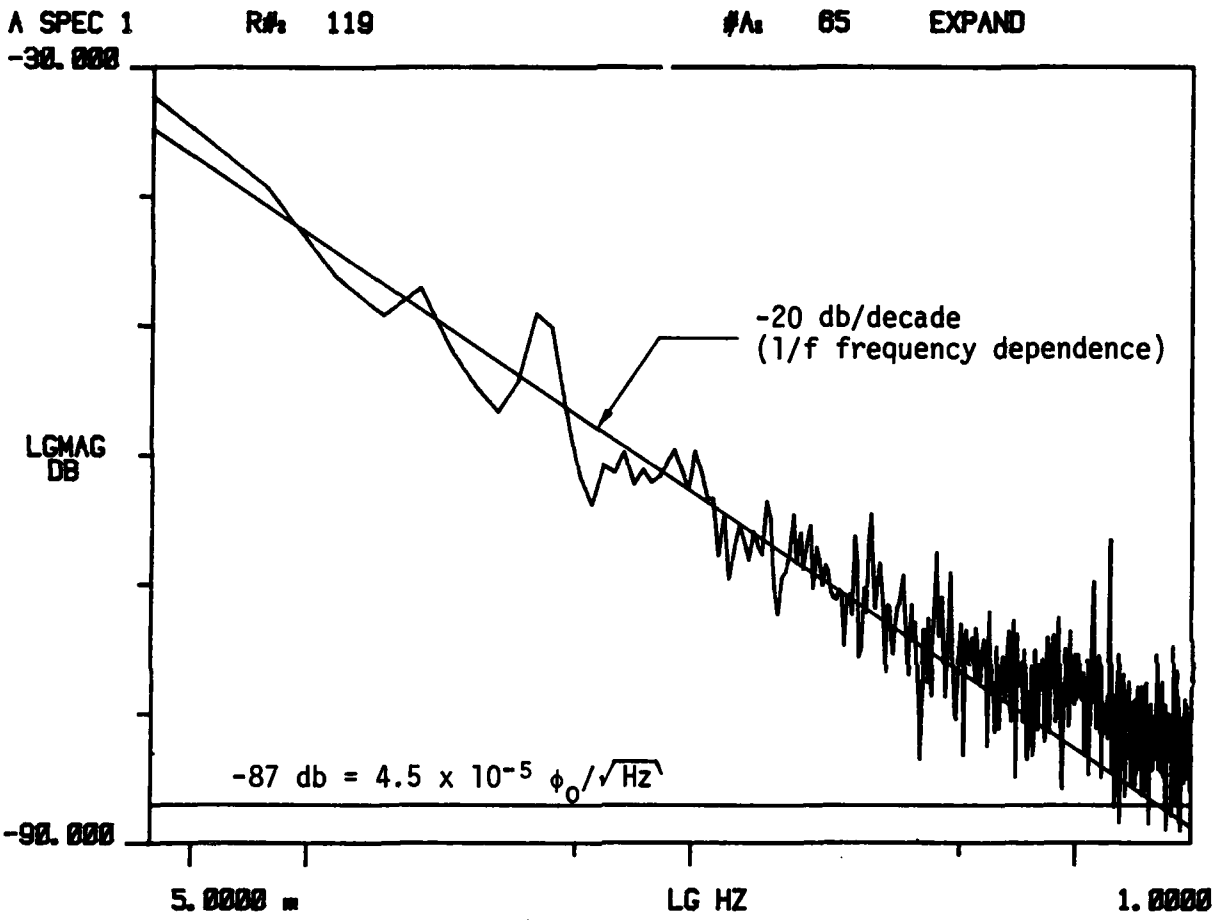

Figure 14. Noise spectrum of dc SQUID measured from 0.005 Hz to 2 Hz. (SQUID #3, substrate #3, made on 8-24-82)

significantly from what it would be if the SQUID were always biased at points of maximum $dv/d\phi$. This should account for the slightly higher white noise level in Figure 13 of $4.5 \times 10^{-5}\ \phi_0/\sqrt{Hz}$.

Gradiometer design.

A design was completed of a gradiometer with one-inch square pickup loops, a baseline of 1.1 inches, and a 50-turn input coil, which will fit on a 3-inch diameter silicon wafer. Figure 15 shows the pickup loops, SQUID, and bias and modulation leads. Figure 16 shows a detailed drawing of the end of the SQUID containing the junctions. A few 5-μm lines of the 50-turn input coil are also shown. Two cross-type junctions 2.5 μm square and four dumbbell-shaped resistors, each five squares long, are shown. Two resistors are associated with each junction. The SQUID is fabricated on a superconducting niobium ground plane in order to achieve a low SQUID inductance and obtain good initial balance. The ground plane extends under the center part of the pickup loops to eliminate balance problems in that area. The ground plane itself is used as part of the pickup loop circuit and provides the return path for current in the circuit formed by the pickup loops and input coil. This minimizes the number of metallization layers needed to fabricate the gradiometer.

The values of the SQUID inductance, input-coil inductance, and input-coil coupling constant depend on the insulator thicknesses chosen. Expected values are approximately 30 pH for the SQUID inductance, 200 nH for the input-coil inductance, and 0.6 for the coupling constant ($M = k\sqrt{L_S L_I}$). The pickup-loop inductance should also be approximately 200 nH. Since this SQUID has a much lower inductance than the 0.9 nH SQUIDs built during this contract,

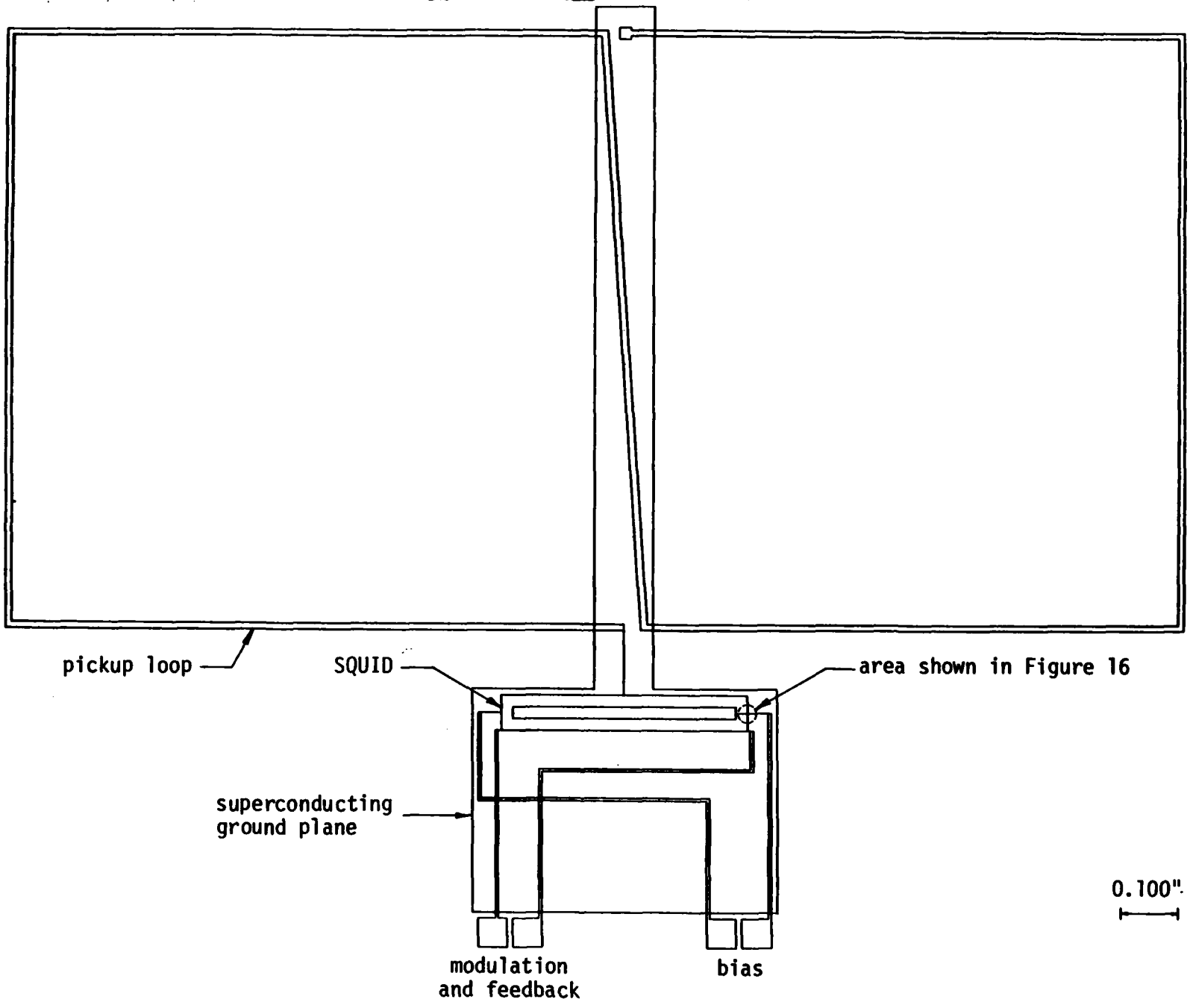

Figure 15. Drawing of gradiometer with one-inch square pickup loops, 50-turn planar input coil, and dc SQUID.

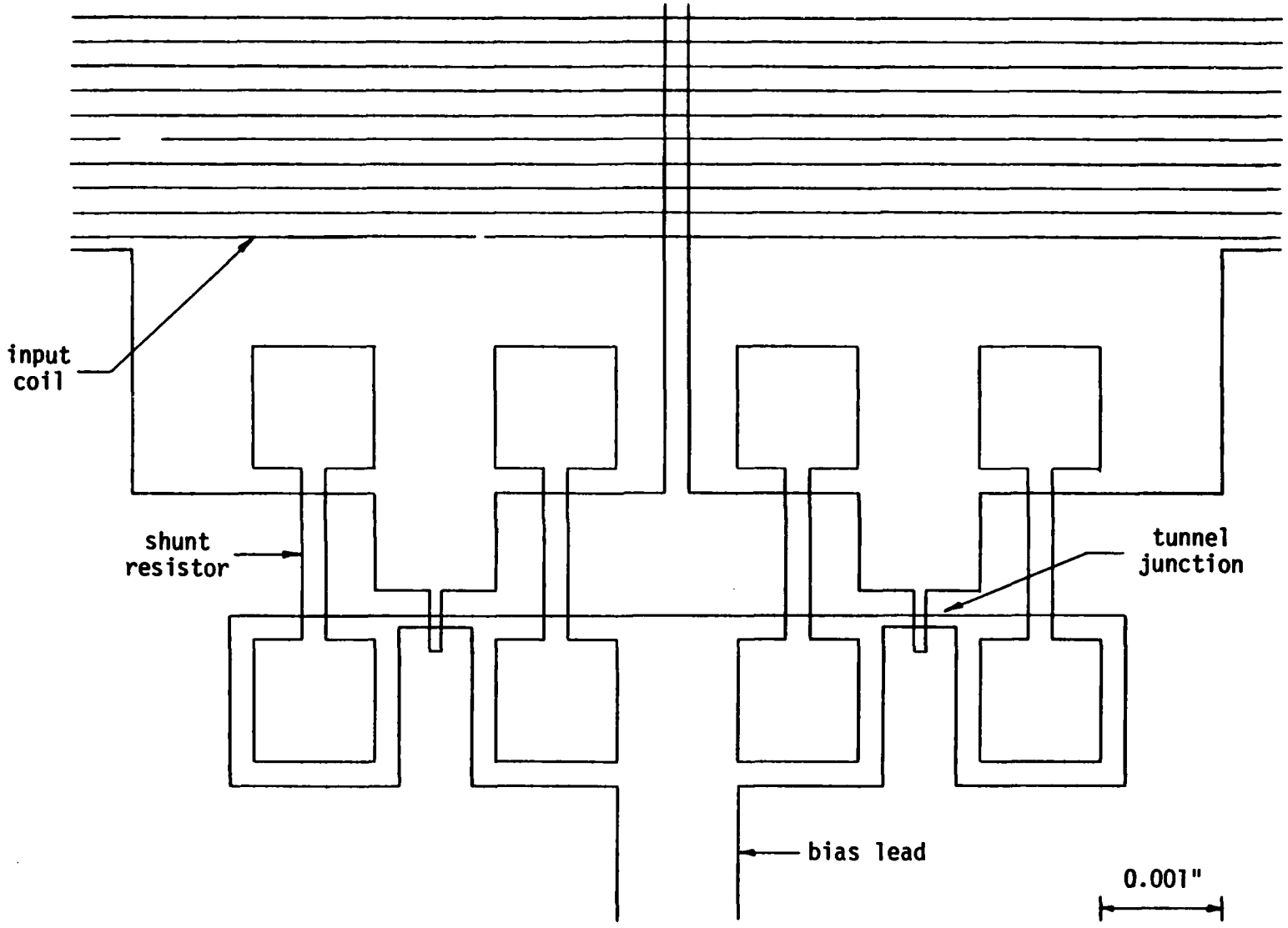

Figure 16. Drawing of end of dc SQUID containing Josephson tunnel junctions and resistive shunts.

the flux noise should be much lower. A simple theory of thermal noise in dc SQUIDs shows that the thermal flux noise should have a spectral density proportional to the square of the inductance of the SQUID, if other parameters are held constant. Using these numbers the predicted sensitivity of this gradiometer is approximately 3×10^{-14} (T/m)/$\sqrt{\text{Hz}}$ = 3×10^{-5} (γ/m)/$\sqrt{\text{Hz}}$. Additional sensitivity can be obtained by using larger substrates and increasing the size of the pickup loops.

Conclusions and recommendations.

Niobium-niobium cross-type tunnel junctions have been made with two different tunnel-barrier materials, aluminum oxide and silicon oxide. The best R_S/R_n ratios obtained for these junctions have been 3.92 for the aluminum-oxide barriers and 4.45 for silicon oxide. Titanium resistive shunts of approximately 10 ohms have been added to these junctions to give nonhysteretic I-V curves. Dc SQUIDs with 2.5 μm square niobium-aluminum oxide-niobium junctions have been fabricated. The SQUID inductance was 0.9 nH. With the SQUIDs operated in a small-signal amplifier mode measurements of the SQUID voltage v, $dv/d\phi$, dv/di, and noise voltage v_n were made as a function of flux ϕ. The white noise of the SQUIDs was measured to have a minimum value of 2.8×10^{-5} $\phi_0/\sqrt{\text{Hz}}$ at 20 kHz in this mode. Low-frequency noise was measured from 0.005 to 2 Hz with the SQUID operated in a closed-loop negative-feedback mode. The white noise measured in this mode was slightly higher than that measured with the feedback loop open. A straight line with a slope of -20 db/decade (1/f frequency dependence) fits the data below 0.5 Hz. This line intersects a horizontal line through the white noise at about 1.6 Hz.

A design was completed of a thin-film gradiometer with one-inch square pickup loops, a baseline of 1.1 lines, and a 50-turn input coil, which will fit on a 3-inch diameter silicon wafer. The sensitivity of this gradiometer was predicted to be 3×10^{-14} (T/m)/$\sqrt{\text{Hz}}$ = 3×10^{-5} (γ/m)/$\sqrt{\text{Hz}}$. Fabrication of this completely integrated gradiometer made only of refractory metals should provide an excellent means of evaluating a thin-film gradiometer for airborne use. It is recommended that this gradiometer should be built and that the following measurements should be made:

(a) coupling of pickup loops to SQUID

(b) white noise levels with the feedback loop open and closed

(c) low-frequency noise

(d) intrinsic balance

(e) hysteresis of gradiometer output when the gradiometer is rotated in opposite directions in the earth's magnetic field

(f) effects of thermal cycling from room temperature to liquid helium temperature

(g) storage characteristics

(h) reproducibility

These devices should enable one to determine if flux noise in thin-film pickup loops is a problem. Also, accurate projections of sensitivities for gradiometers with larger pickup loops should be able to be made.

References.

1. V. Ambegaokar and A. Baratoff, Phys. Rev. Lett. 10, 486 (1963); 11, 104 (1963).

2. G. Paterno, P. Rissman, and R. Vaglio, J. Appl. Phys. 46, 1419 (1975).

3. T. Van Duzer and C. W. Turner, Principles of Superconductive Devices and Circuits (Elsevier North Holland, Inc., New York, 1981), p. 87.

4. M. Gurvitch, M. A. Washington, and H. A. Huggins, Appl. Phys. Lett. 42, 472 (1983).

5. R. F. Broom, S. I. Raider, A. Oosenbrug, R. E. Drake, and W. Walter, IEEE Trans. Elect. Dev. ED-27, 1998 (1980).

6. H. Kroger, L. N. Smith, and D. W. Jillie, Appl. Phys. Lett. 39, 280 (1981).


4-
DT